Motion and Switching of Dual-Vortex Cores in Elliptical Permalloy Nanodisk Stimulated by a Gaussian Magnetic Field Pulse

X. Li[1], Y. Zhou[2], T. Zeng[1], K.-W. Lin[3], P. T. Lai[1], and Philip W. T. Pong[1]

[1]Department of Electrical and Electronic Engineering, The University of Hong Kong, Hong Kong
[2]School of Science and Engineering, The Chinese University of Hong Kong, Shenzhen 518172, China
[3]Department of Materials Science and Engineering, National Chung Hsing University, Taichung 402, Taiwan

Magnetic nanostructures have potential applications in ultrahigh-density magnetic storage. In this paper, the dynamics of the dual magnetic vortices in elliptical Permalloy nanodisk are investigated using micromagnetic modeling. Under the stimulation of the short-axis (*y*-axis) Gaussian field pulse and long-axis (*x*-axis) constant field, the equilibrium positions of dual-vortex cores can be driven away from the initial positions. The displacement in the *y*-direction is proportional to the magnitude of the *x*-axis constant field. The displacement in the *x*-direction exhibit periodic reliance on the pulsewidth of the *y*-axis Gaussian field pulse. The threshold value of pulse strength for dual-vortex motion increases with the magnitude of the *x*-axis constant field. The mechanism of polarity and chirality switching in dual-vortex cores are studied through analyzing the trajectories of vortex cores in the annihilation and nucleation processes. The switching of polarity exhibits an oscillatory dependence on the pulsewidth and strength. The minimum pulse strength required for chirality switching is 120 mT, while the corresponding pulsewidth is influenced by the *x*-axis constant field. This paper provides insights on the magnetization dynamics of nanostructures containing dual vortices subject to external excitations.

Index Terms—**Dual-vortex cores, micromagnetic simulation, vortex-core motion, vortex-core switching.**

I. Introduction

THE exploration of spintronic devices has attracted a great deal of attention, especially in the patterned nanostructures due to the extremely fast response (from femtosecond to nanosecond) to external excitations of nanomagnets. Nanometer- or micrometer-sized thin film elements with magnetic vortex structure (also described as the spin curling structure) are potential candidates for future nonvolatile magnetic memories [1]–[3]. Intense research has been conducted to reveal the static and dynamic properties of magnetic vortices [4]–[12]. The curling structures are formed as the competition among the exchange, magnetostatic, anisotropy, and Zeeman energy [13]. The spins at the center of the magnetic vortex (also described as the vortex core) are perpendicular to the magnetic thin film in order to reduce the exchange energy. The geometrical features of the magnetic vortices are characterized by the polarity $p = \pm 1$ ($p = 1$ stands for up and $p = -1$ for down of the magnetization in the vortex core) and the chirality [$c = 1$ for clockwise (CW) and $c = -13$ for counterclockwise (CCW)] [14].

Single magnetic vortex structures widely appear in square, circular, and elliptical magnetic thin films as ground states. Reports have shown that the single magnetic vortex confined in Permalloy ferromagnetic dots can demonstrate resonant behaviors under in-plane magnetic field at the oscillation frequencies given by the magnetostatic energy [15]–[17]. The single vortex core polarity switching phenomenon in submicrometer magnetic thin film has also been intensively investigated under external excitations, including injected current, magnetic ac field, and magnetic field pulses with both square and Gaussian shapes [5], [6], [18]–[23]. In addition to the interests in single magnetic vortex characterizations, both theoretical and experimental studies have been extended to the interactions between magnetic vortices in a pair of ferromagnetic dots, where each of them contains a single magnetic vortex [24]–[27]. Aside from the above-mentioned topics, the dual vortex structure trapped in the elliptical magnetic thin film is introduced in some reports, which involves the study of magnetization reversal and oscillatory properties [28]–[30] However, the magnetization dynamics of the dual magnetic vortices under magnetic field pulses are not yet reported.

In this paper, we simulated a dual magnetic vortex structure, which is confined in a Permalloy elliptical nanodisk by micromagnetic modeling. Through the combination of a constant magnetic field and an in-plane field pulse, a series of dual magnetic vortex magnetization configurations is observed. It is of interest to find that the magnitude of the static field and the width and strength of the field pulse exhibit decisive influence on the dual magnetic vortex core distribution. Meanwhile, the study on the switching of the polarity and chirality of the dual-vortex cores has also been conducted. This paper helps reveal the mechanisms for multivortex core motion and switching in the magnetic thin films.

II. Micromagnetics Model

The simulation was conducted by the object oriented micromagnetic framework [31]. The micromagnetic modeling is based on the Landau–Lifshitz–Gilbert equation [32], [33]

$$\frac{d\vec{M}}{dt} = -|\gamma|\vec{M} \times \vec{H}_{eff} + \frac{\alpha}{M_s}\left(\vec{M} \times \frac{d\vec{M}}{dt}\right) \quad (1)$$

Manuscript received July 18, 2016; revised September 21, 2016; accepted January 4, 2017. Date of publication January 9, 2017; date of current version April 17, 2017. Corresponding authors: Y. Zhou (e-mail: zhouyan@cuhk.edu.cn); P. W. T. Pong (e-mail: ppong@eee.hku.hk).

Color versions of one or more of the figures in this paper are available online at http://ieeexplore.ieee.org.

Digital Object Identifier 10.1109/TMAG.2017.2650151

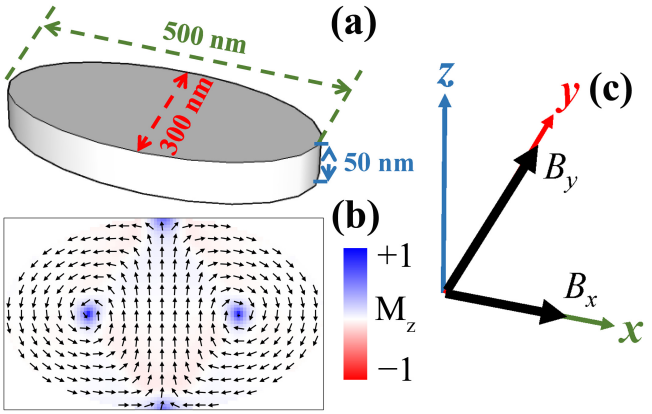

Fig. 1. (a) Schematic of the elliptical thin-film structure. (b) Magnetization configurations of the elliptical thin film with a dual vortex configuration. (c) Directions of B_x and B_y in the coordinate system.

where $\gamma = 2.09 \times 10^{11}$ rad·Hz·T^{-1} denotes the gyromagnetic ratio, $\alpha = 0.05$ denotes the damping parameter, and $M = 860$ emu/cm^3 denotes the saturation magnetization, respectively. H_{eff} is the effective field calculated as the summation of external magnetic field and exchange interaction field. Magnetocrystalline anisotropy constant of $K = 0$ and exchange constant of $A_{\text{ex}} = 1.3 \times 10^{-6}$ erg/cm (typical for Permalloy) are used [18]. An elliptical element with medium aspect ratio presents a reversal mechanism of dual-vortex nucleation and annihilation [34]. The geometrical parameters are thus defined as the long axis of 500 nm, the short axis of 300 nm, and the thickness of 50 nm [Fig. 1(a)]. The elliptical nanodisk is discretized into cubes with the dimensions of $5 \times 5 \times 5$ nm^3. The magnetization of the cubes in the center of the layer (height of 25–30 nm) is considered in the discussion to avoid the influence of the edge effect. The magnetization of the nanodisk is firstly set to be uniformly aligned perpendicular to the plane. A magnetic field (80 mT) is subsequently applied along the short axis to saturate the system. The field is gradually decreased to 0 mT and the system nucleates into a symmetric dual vortex geometry [Fig. 1(b)]. This dual-vortex geometry is typical of the remnant state in a thick submicrometer NiFe dot, as proved by previous micromagnetic simulations and experimental observations [29], [35], [36].

After the dual-vortex geometry is formed, a static magnetic field (B_x) is applied in the $+x$-direction [Fig. 1(c)]. The dual-vortex cores are displaced symmetrically to the third quadrant (the left core) and the first quadrant (the right core). The vortex cores reach new equilibrium positions after relaxation. This magnetization configuration is used as the initial status at $t = 0$ ns. Magnetic field pulse was applied at (B_y) is superimposed to the elliptical thin film to stimulate the motion of the dual-vortex cores. According to the simulation, both Gaussian pulses and square-shaped pulse are effective to stimulate the vortex dynamics. In this paper, Gaussian field pulse is adopted as an example

$$B_y(t) = \begin{cases} S_{pulse} e^{-(t-2\sigma)^2/2\sigma^2} & 0 \le t \le 4\sigma \\ 0 & t > 4\sigma \end{cases} \quad (2)$$

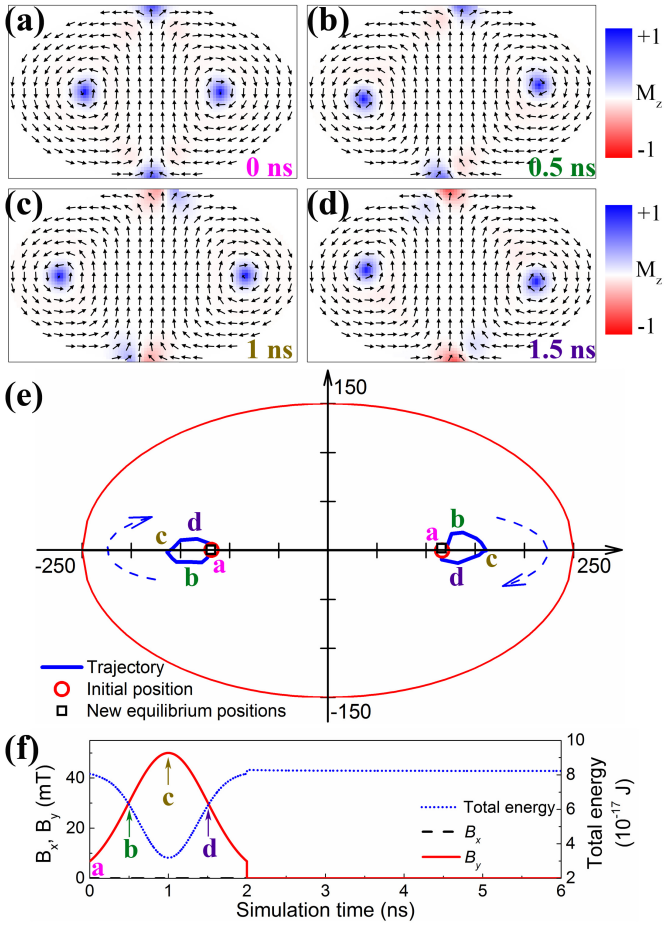

Fig. 2. Dynamics of the dual-vortex cores under field pulse ($S_{\text{pulse}} = 50$ mT and FWHM $= 1.18$ ns) when $B_x = 0$: magnetization configuration when (a) $t = 0$ ns, (b) $t = 0.5$ ns, (c) $t = 1$ ns, and (d) $t = 1.5$ ns. (e) Trajectories of the motion of vortex cores and (f) B_x, B_y (left axis), and total energy (right axis) as a function of simulation time.

where S_{pulse} stands for the pulse strength, and σ stands for the standard deviation [the full width at half maximum (FWHM) is calculated as $2\sqrt{2\ln 2}\sigma \approx 2.355\sigma$]. The center of the pulse is maintained at $t = 2\sigma$, $S_{\text{pulse}} = 20$ mT–150 mT, and $\sigma = 200$–1000 ps (FWHM $= 0.47$ ns–2.36 ns) are used in the simulations.

III. Results and Discussion

The above-mentioned simulations have shown that stable and symmetric dual magnetic vortex geometry can be formed at the remnant state. We further study the magnetization dynamics of the dual-vortex cores by applying a y-axis Gaussian field pulse under constant *x-axis* field. Through changing the parameters, including B_x, FWHM, and S_{pulse}, the motion and switching of the dual-vortex cores are observed.

A. Dynamics of Dual-Vortex Cores Under Field Pulse

In order to explore how the nanodisk react to external excitations, the time evolution of the dual-vortex cores stimulated by a y-direction Gaussian field pulse ($S_{\text{pulse}} = 50$ mT and FWHM $= 1.18$ ns) is investigated. In the case of zero x-axis field, the dual vortices are symmetrically distributed on the x-axis at $t = 0$ ns [Fig. 2(a)]. As B_y gradually increases,

the left core is driven to the third quadrant, while the right one to the first quadrant. The displacement in the y-direction is largest at $t = 0.5$ ns, and is gradually reduced back to zero with increasing B_y. This is explained by the elliptical trajectories of the vortex core motions with the periods of 2 ns. The vortex cores reach the minor axes after 0.5 ns (i.e., 1/4 of the period). At $t = 1$ ns, the separation between the two vortex cores is largest in the x-direction [Fig. 2(c)] as B_y reaches the maximum. During the trailing edge of the pulse, the vortex cores gyrate to the second quadrant (left core) and the fourth quadrant (right core) [Fig. 2(d)]. The trajectories of the dual-vortex core motion are plotted by capturing the time evolution of the vortex core positions with a time interval of 0.3 ns [Fig. 2(e)]. The left core gyrates CW, while the right one moves anticlockwise. This direction is primarily determined by the direction of B_y. The time evolution of the magnetization is driven by the changes of total energy shown in Fig. 2(f). When $t < 2$ ns, the total energy changes with B_y, and is minimum when B_y is largest. After B_y dies down, the total energy gradually relaxes to the minimum value as the vortex cores return to their initial equilibrium positions [Fig. 2(f)].

When the dual-vortex cores are relaxed by a small x-axis constant field ($B_x = 8$ mT), the left core is driven to the second quadrant, and the right one to the fourth quadrant, as shown in Fig. 3(a). This shift in the y-direction enlarges the area that is parallel to B_x and reduces the area that is antiparallel to minimize the Zeeman energy [37], [38]. When the field pulse is applied ($S_{\text{pulse}} = 50$ mT and FWHM $= 1.18$ ns) in the $+y$-direction, the vortex cores gyrate CW to the new equilibrium positions. The magnetization configurations at $t =$ 0.5, 1, and 1.5 ns are shown in Fig. 3(b)–(d), respectively. However, unlike in Fig. 2, where the magnetization resumes its initial configuration after the field pulse, the dual-vortex cores find new equilibrium positions after relaxation when $B_x = 8$ mT [Fig. 3(e)]. Both vortex cores are shifted to the right of their initial positions. This asymmetric shift of vortex cores after the short-axis field pulse is also observed in a previous report [39]. The changes in the equilibrium positions can be interpreted by the transition between different energy states [Fig. 3(f)]. Several magnetization configurations may present local minimum of magnetic energy, since the symmetry is broken by B_x. Before the application of B_y, the system exhibits a global ground state with the total energy of 7.90×10^{-17} J. At $t = 2$ ns, and the total energy was increased to 8.1×10^{-17} J after the excitation of the field pulse. After relaxation, the system approaches a metastable state with the local minimum energy of 7.92×10^{-17} J. The y-axis field pulse acts on the system to overcome the energy barrier ($\sim 2 \times 10^{-18}$ J) between different minimum-energy configurations. This energy barrier is higher than the thermal energy at room temperature (4.1×10^{-21} J), indicating high resistance to thermal or defect-induced fluctuations. The displacement of both vortex cores is nearly the same, so that the total magnetization in the y-direction remains small when B_y drops to zero. The above-mentioned results indicate that the y-axis field pulse is a promising method to alter the positions of the dual-vortex cores.

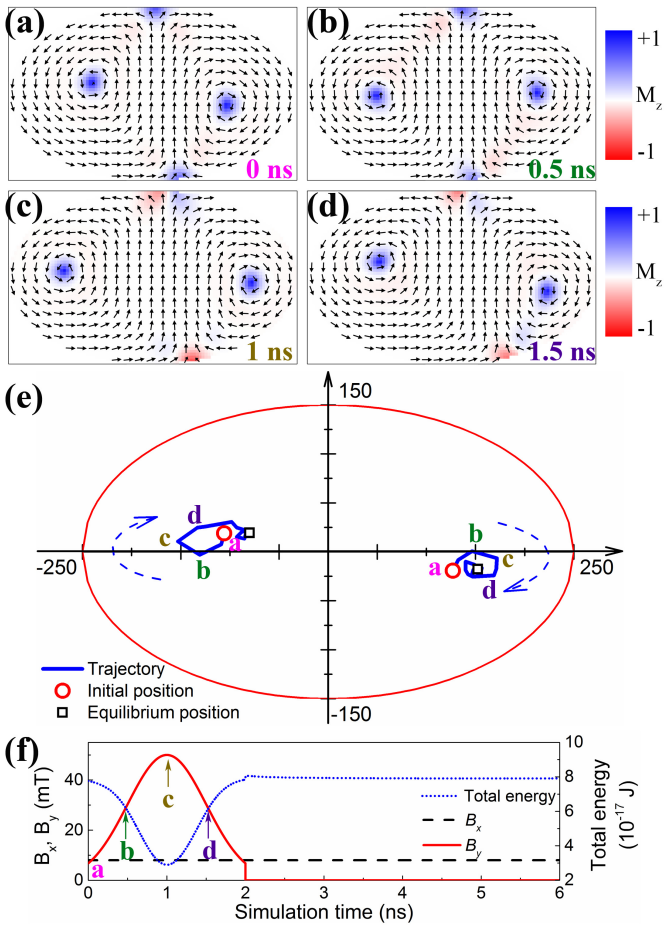

Fig. 3. Dynamics of the dual-vortex cores under field pulse ($S_{\text{pulse}} = 50$ mT and FWHM $= 1.18$ ns) when $B_x = 8$ mT: magnetization configuration when (a) $t = 0$ ns, (b) $t = 0.5$ ns, (c) $t = 1$ ns, and (d) $t = 1.5$ ns. (e) Trajectories of the motion of vortex cores and (f) B_x, B_y (left axis), and total energy (right axis) as a function of simulation time.

B. Motion of the Equilibrium Positions of Dual-Vortex Cores

To evaluate how the displacements of the vortex cores can be influenced by the profile of external excitations, the evolution of the magnetization of an elliptical thin film is investigated under different constant magnetic field and pulse field.

The influence of pulsewidth is investigated while maintaining S_{pulse} at 50 mT. When a small x-axis constant field ($B_x = 6$ mT) is applied, the displacement of vortex cores is within 10 nm regardless of the pulsewidth [Fig. 4(a)]. When larger B_x of 8 mT is applied, the new equilibrium positions of the dual-vortex cores exhibit periodic changes along the x-direction as FWHM is changed from 0.47 to 2.36 ns [Fig. 4 (b)]. When the pulsewidth is set to be 0.47 ns [A in Fig. 4(b)], the dual-vortex cores are displaced by 27 nm to the right of their initial positions. At larger pulsewidth of 0.7 ns [B in Fig. 4(b)], the maximum displacement of 54 nm is achieved to the right of the initial positions. However, as the pulsewidth increases to 1.41 ns [D in Fig. 4(b)], the dual cores are driven to the left of their initial positions with a maximum displacement of 22 nm. When FWHM $=$ 2.36 ns [F in Fig. 4(b)], the new equilibrium positions of dual-vortex cores resume the positions of FWHM $= 0.47$ ns. The

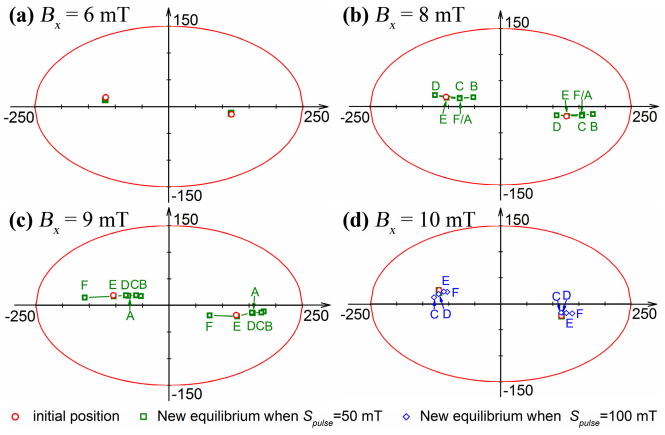

Fig. 4. Equilibrium positions of dual-vortex cores before and after the 50 mT (green square) or 100 mT (blue diamond) y-axis Gaussian field pulse with FWHM ranging from 0.47 to 2.36 ns under the x-axis constant field of (a) 6, (b) 8, (c) 9, and (d) 10 mT (A–F refer to the new equilibrium positions of vortex cores when FWHM equals to A: 0.47 ns, B: 0.71 ns, C: 0.94 ns, D: 1.41 ns, E: 1.88 ns, and F: 2.36 ns).

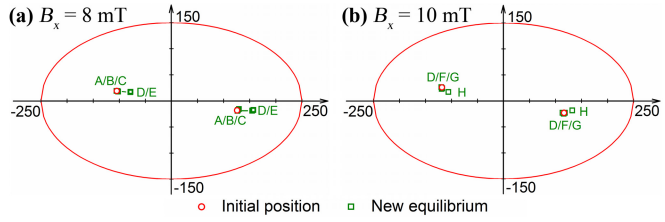

Fig. 5. Equilibrium positions of dual-vortex cores before and after the y-axis Gaussian field pulse with S_{pulse} ranging from 20 to 100 mT under x-axis constant field of (a) 8 and (b) 10 mT (A–G refer to the new equilibrium positions of vortex cores when S_{pulse} equals to A: 20 mT, B: 30 mT, C: 40 mT, D: 50 mT, E: 60 mT, F: 70 mT, G: 80 mT, and H: 90 mT).

pulsewidth dependence can be explained by the gyration of the vortices around their equilibrium positions. The dependence of the displacement on pulsewidth is attributed to the different distances of the gyroscopic motion during the field pulse. The corresponding energies for configurations A–F in Fig. 4(b) are 7.90×10^{-17} J, 7.92×10^{-17} J, 7.92×10^{-17} J, 7.92×10^{-17} J, and 7.91×10^{-17} J, respectively, which are all relatively larger than the energy of 7.90×10^{-17} J at initial state. Similar pulsewidth dependence is also observed when $B_x = 9$ mT [Fig. 4(c)], while the displacement is larger. However, when B_x is further increased to 10 mT, the vortex cores only move within a small region of 10 nm as FWHM is changed from 0.47 to 2.36 ns [Fig. 4(d)]. However, noticeable displacements of vortex cores are observed when stronger field pulse is applied ($S_{\text{pulse}} = 100$ mT).

In order to further investigate the influence of pulse strength, the initial and new equilibrium positions of dual-vortex cores subject to the y-axis Gaussian field pulse of different strength and the same FWHM of 1.18 ns are shown in Fig. 5. When $B_x = 8$ mT, the displacements of the vortex cores are not obvious until S_{pulse} is higher than 50 mT [Fig. 5(a)]. This is because the weak field pulse is not sufficient to overcome the energy barriers between different energy states with local minima. When S_{pulse} is large enough, the cores relax into a local (metastable) state different from the initial state.

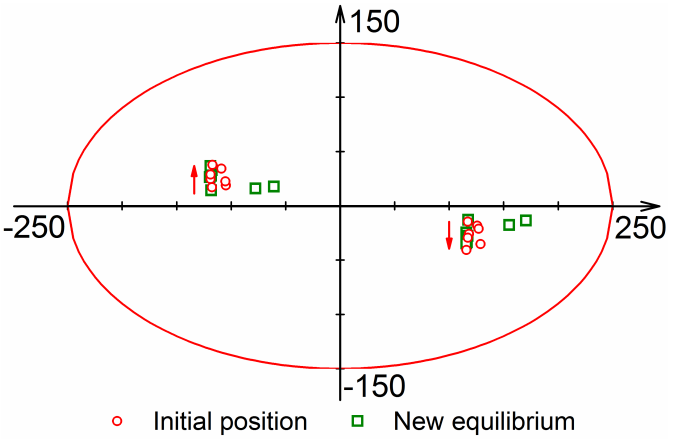

Fig. 6. Equilibrium positions of dual-vortex cores before and after the y-axis Gaussian field pulse with S_{pulse} of 50 mT and σ of 500 ps when B_x is changed from 6 to 16 mT (from the beginning to the end of the arrows, B_x is 6, 8, 9, 10, 12, 14, and 16 mT, respectively)

The threshold S_{pulse} for vortex core motion is increased to 90 mT at higher B_x of 10 mT [Fig. 5(b)]. As such, $S_{\text{pulse}} = 50$ mT results in no displacement of the equilibrium positions, while $S_{\text{pulse}} = 100$ mT shifts the vortex cores remarkably in Fig. 4(d).

The above discussions show that the x-axis constant field is required for the motion of vortex cores. The dependence of the displacement on B_x is further studied. As B_x is increased from 6 to 16 mT, the initial positions of the dual-vortex cores are driven farther away from the x-axis (Fig. 6). This is consistent with the previous results that the dual vortices can be separated along the short-axis through applying long axis field in Permalloy elliptical elements [29]. Under the stimulation of the Gaussian field pulse ($S_{\text{pulse}} = 50$ mT and FWHM = 1.18 ns), the dual-vortex cores are shifted along the x-direction when $B_x = 8$ and 9 mT. The small displacements (< 5 nm) for other B_x values are due to the lack of asymmetry under smaller B_x, or to the smaller pulse strength than the threshold value under larger B_x, as discussed in Figs. 4 and 5.

The above-mentioned results reveal that the new equilibrium positions of the vortex cores can be distributed along the x-direction by adjusting the pulsewidth and strength of the y-axis Gaussian pulse field and can be shifted along the y-direction by changing the magnitude of the constant$x$-axis field. This provides an effective method in manipulating the position of the dual-vortex cores in the elliptical thin film elements.

C. Switching of Polarity and Chirality of Dual-Vortex Cores

As discussed in Sections III-A and III-B, the Gaussian field pulse can excite the motion of the dual-vortex cores. When the strength of the field pulse is further increased, the dual-vortex cores start to switch, which results in the changes in polarity or chirality. The trajectory of the dual-vortex core motion excited by a y-axis Gaussian field pulse ($S_{\text{pulse}} = 110$ mT and FWHM = 1.18 ns) under B_x of 10 mT is shown in Fig. 7(a). At $t = 0$ ns, the vortex cores ($c = -1$ and $p = 1$ for the left core, and $c = 1$ and $p = 1$ for the right core) are distributed at the second (left core) and fourth (right core) quadrants. The vortices are driven to the annihilation point

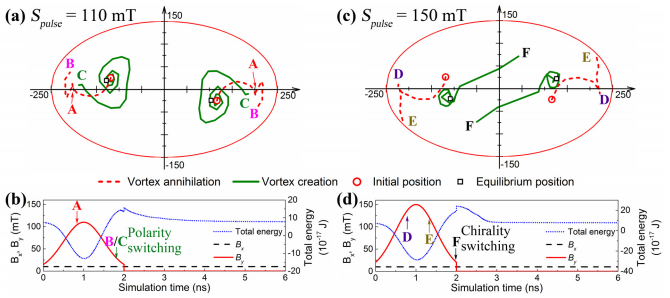

Fig. 7. Dynamics of the dual vortex (a) and (b) polarity and (c) and (d) chirality switching under field pulse (FWHM = 1.18 ns) when $B_x = 10$ mT: trajectories of the annihilation (dashed line) and creation (solid line) of dual-vortex cores subject to field pulse of (a) $S_{\text{pulse}} = 110$ mT and (c) $S_{\text{pulse}} = 150$ mT, and B_x, B_y (left axis), and total energy (right axis) as a function of simulation time when (b) $S_{\text{pulse}} = 110$ mT and (d) $S_{\text{pulse}} = 150$ mT.

[B in Fig. 7(a)] by the strong field pulse, and a new dual-vortex pair with the same chirality but the opposite polarity is nucleated at $t = 1.8$ ns [C in Fig. 7(a)]. As B_y gradually drops to zero, the new dual-vortex cores gyrate CCW toward the new equilibrium positions. At $t = 6$ ns, the total energy drops to the minimum value [Fig. 7 (b)], and the system is relaxed into a new equilibrium state ($c = -1$ and $p = -1$ for the left core, and $c = 1$ and $p = -1$ for the right core). Further increasing the pulse strength to 150 mT while maintaining the pulsewidth at 1.18 ns results in changes in chirality [Fig. 7(c) and (d)]. The high pulse strength results in a larger radius of gyration and thus higher velocity in the vortex core motion. At $t = 1.3$ [E in Fig. 7(c)], the vortex cores are expelled out of the ellipse and the magnetization is saturated along the $+y$-direction. As B_y gradually decreases, the magnetization evolves into a C-like curved state at $t = 1.4$ ns. When the field pulse has passed, new dual-vortex cores with the opposite chirality ($c = 1$ and $p = 1$ for the left core, and $c = -1$ and $p = 1$ for the right core) are created in the first and third quadrant [F in Fig. 7(c)]. The dual cores quickly move to the third and first quadrant, respectively, and finally gyrate to the new equilibrium positions. From Fig. 7(d), one can conclude that the motion of vortex cores is driven by the reduction of total energy.

The diagrams of the dual-vortex switching when $B_x = 6$ and 10 mT are shown in Fig. 8(a) and (b), respectively. The annihilation and formation processes of the left and right vortex cores are symmetric. The geometrical features of the left vortex are discussed here, since the left and right vortex core exhibit the same polarity and the opposite chirality. An oscillation of polarity switching with the pulse strength is observed. The spins of vortex cores are pointed upward at the initial state. The y-axis Gaussian field pulse of $S_{\text{pulse}} = 100$ mT and FWHM = 1.41 ns can switch the pole to downward. As S_{pulse} is increased to 120 mT, no polarity switching is observed. However, further increasing S_{pulse} to 130 mT changes the polarity to downward again. This oscillatory behavior is consistent with the previous report on the single vortex switching in elliptical disks [22]. The oscillatory characteristics of the polarity switching with the pulse strength and pulsewidth resulted from the oscillating displacements of vortex cores at the end of the field pulse [19]. Since the velocity of vortex core is proportional to the distance

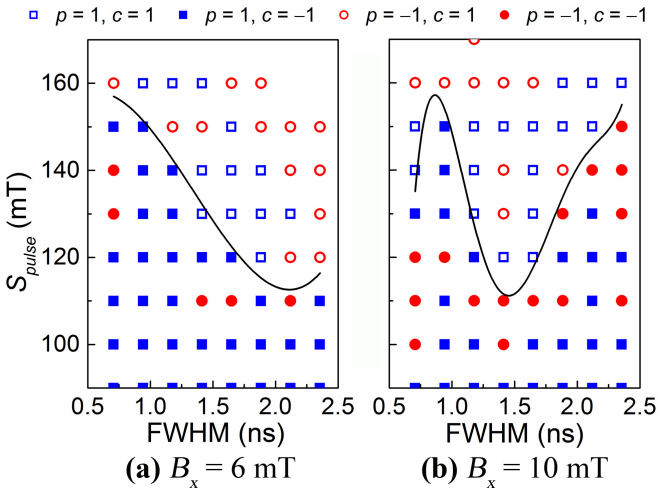

Fig. 8. Diagram of the polarity and chirality of the left vortex core versus pulselength and pulse strength for (a) $B_x = 6$ mT and (b) $B_x = 10$ mT.

from the new equilibrium position, the vortex core that is farthest from the equilibrium has higher velocity to reach the critical value for polarity switching.[22], [40]. The solid lines in Fig. 8(a) and (b) distinguish the regions of chirality switching from the unswitched regions. The minimum S_{pulse} required for the chirality change is 120 mT for $B_x = 6$ and 10 mT, while the minimum points correspond to different pulsewidth of 2.12 and 1.41 ns, respectively. This indicates that B_x influences the chirality switching by changing the position of annihilation point through influencing the initial core position. These results show that the polarity and chirality of the dual-vortex cores can be manipulated through applying a Gaussian field pulse with different pulse strengths and pulsewidths.

IV. Conclusion

In conclusion, the motion and the switching of the dual-vortex cores in an elliptical thin film are observed by manipulating the magnitude of the x-axis constant field and the profile of the y-axis Gaussian pulse field. When no x-axis field is applied, the dual-vortex cores gyrate back to the initial position after the field pulse. However, B_x breaks the symmetry, and hence, the displacements of the dual-vortex cores are excited by the field pulse. The threshold value of S_{pulse} for vortex motion is increased at larger B_x. The shift along the x-direction is dependent on S_{pulse} and FWHM of the field pulse, while the motion in the y-direction is dominated by B_x. The switching of the vortex polarity exhibits oscillatory reliance on S_{pulse} and FWHM. At higher S_{pulse}, the vortex cores are expelled out of the ellipse, and the change in chirality is observed in the newly formed vortex cores. These results are potentially useful for studying the dynamics of the dual magnetic vortex structure in the elliptical thin film, which is also beneficial for the application of multivortices in next-generation memory devices.

Acknowledgment

This work was supported in part by the Seed Funding Program for Basic Research, Seed Funding Program for

Applied Research, and Small Project Funding Program from the University of Hong Kong, ITF Tier 3 funding under Grant Nos. ITS/203/14, ITS/104/13, and ITS/214/14, in part by the RGC-GRF under Grant No. HKU 17210014, and in part by the University Grants Committee of Hong Kong under Contract No. AoE/P-04/08. The work of Y. Zhou was supported in part by the National Natural Science Foundation of China under Project No. 11574137 and in part by the Shenzhen Fundamental Research Fund under Grant No. JCYJ20160331164412545.

REFERENCES

[1] N. Nishimura *et al.*, "Magnetic tunnel junction device with perpendicular magnetization films for high-density magnetic random access memory," *J. Appl. Phys.*, vol. 91, no. 8, pp. 5246–5249, Apr. 2002.

[2] C. A. Ross, "Patterned magnetic recording media," *Annu. Rev. Mater. Res.*, vol. 31, no. 1, pp. 203–235, 2001.

[3] A. Wachowiak, J. Wiebe, M. Bode, O. Pietzsch, M. Morgenstern, and R. Wiesendanger, "Direct Observation of Internal Spin Structure of Magnetic Vortex Cores," *Science*, vol. 298, no. 5593, pp. 577–580, Oct. 2002.

[4] Y. Chen *et al.*, "Quasi-one-dimensional miniature multiferroic magnetic field sensor with high sensitivity at zero bias field," *Appl. Phys. Lett.*, vol. 99, no. 4, p. 042505, Jul. 2011.

[5] Q. F. Xiao, J. Rudge, B. C. Choi, Y. K. Hong, and G. Donohoe, "Dynamics of vortex core switching in ferromagnetic nanodisks," *Appl. Phys. Lett.*, vol. 89, no. 26, p. 262507, Dec. 2006.

[6] R. Hertel, S. Gliga, M. Fähnle, and C. M. Schneider, "Ultrafast nanomagnetic toggle switching of vortex cores," *Phys. Rev. Lett.*, vol. 98, no. 11, p. 117201, Mar. 2007.

[7] V. Uhlir *et al.*, "Dynamic switching of the spin circulation in tapered magnetic nanodisks," *Nature Nanotechnol.*, vol. 8, no. 5, pp. 341–346, May 2013.

[8] Y.-S. Yu *et al.*, "Resonant amplification of vortex-core oscillations by coherent magnetic-field pulses," *Sci. Rep.*, vol. 3, p. 1301, Feb. 2013.

[9] J. Raabe, R. Pulwey, R. Sattler, T. Schweinböck, J. Zweck, and D. Weiss, "Magnetization pattern of ferromagnetic nanodisks," *J. Appl. Phys.*, vol. 88, no. 7, pp. 4437–4439, Oct. 2000.

[10] T. Shinjo, T. Okuno, R. Hassdorf, K. Shigeto, and T. Ono, "Magnetic vortex core observation in circular dots of permalloy," *Science*, vol. 289, no. 5481, pp. 930–932, Aug. 2000.

[11] S.-B. Choe *et al.*, "Vortex core-driven magnetization dynamics," *Science*, vol. 304, no. 5669, pp. 420–422, Apr. 2004.

[12] B. Van Waeyenberge *et al.*, "Magnetic vortex core reversal by excitation with short bursts of an alternating field," *Nature*, vol. 444, no. 7118, pp. 461–464, Nov. 2006.

[13] K. Y. Guslienko, B. A. Ivanov, V. Novosad, Y. Otani, H. Shima, and K. Fukamichi, "Eigenfrequencies of vortex state excitations in magnetic submicron-size disks," *J. Appl. Phys.*, vol. 91, no. 10, pp. 8037–8039, May 2002.

[14] M. Jaafar *et al.*, "Control of the chirality and polarity of magnetic vortices in triangular nanodots," *Phys. Rev. B, Condens. Matter*, vol. 81, no. 5, p. 054439, Feb. 2010.

[15] Y. Acremann *et al.*, "Imaging precessional motion of the magnetization vector," *Science*, vol. 290, no. 5491, pp. 492–495, Oct. 2000.

[16] J. P. Park, P. Eames, D. M. Engebretson, J. Berezovsky, and P. A. Crowell, "Imaging of spin dynamics in closure domain and vortex structures," *Phys. Rev. B, Condens. Matter*, vol. 67, no. 2, p. 020403, Jan. 2003.

[17] J. Raabe, C. Quitmann, C. H. Back, F. Nolting, S. Johnson, and C. Buehler, "Quantitative analysis of magnetic excitations in Landau flux-closure structures using synchrotron-radiation microscopy," *Phys. Rev. Lett.*, vol. 94, no. 21, p. 217204, Jun. 2005.

[18] R. Antos and Y. Otani, "Simulations of the dynamic switching of vortex chirality in magnetic nanodisks by a uniform field pulse," *Phys. Rev. B, Condens. Matter*, vol. 80, no. 14, p. 140404, Oct. 2009.

[19] M. Weigand *et al.*, "Vortex core switching by coherent excitation with single in-plane magnetic field pulses," *Phys. Rev. Lett.*, vol. 102, no. 7, p. 077201, Feb., 2009.

[20] J.-S. Yang, C.-M. Lee, and C.-R. Chang, "Switching behavior of vortex cores in bilayer nanodots by uniform magnetic field pulses," *IEEE Trans. Magn.*, vol. 47, no. 3, pp. 641–644, Mar. 2011.

[21] M. Kammerer *et al.*, "Magnetic vortex core reversal by excitation of spin waves," *Nature Commun.*, vol. 2, p. 279, Apr. 2011.

[22] Y. Keisuke *et al.*, "Switching of magnetic vortex core in elliptical disks by nanosecond field pulses," *Appl. Phys. Exp.*, vol. 7, no. 6, p. 063008, Jun. 2014.

[23] G. Lv, H. Zhang, X. Cao, F. Gao, and Y. Liu, "Micromagnetic simulations of magnetic normal modes in elliptical nanomagnets with a vortex state," *Appl. Phys. Lett.*, vol. 103, no. 25, p. 252404, Dec. 2013.

[24] X. M. Cheng, K. S. Buchanan, R. Divan, K. Y. Guslienko, and D. J. Keavney, "Nonlinear vortex dynamics and transient domains in ferromagnetic disks," *Phys. Rev. B, Condens. Matter*, vol. 79, no. 17, p. 172411, May 2009.

[25] J. Shibata, K. Shigeto, and Y. Otani, "Dynamics of magnetostatically coupled vortices in magnetic nanodisks," *Phys. Rev. B, Condens. Matter*, vol. 67, no. 22, p. 224404, Jun. 2003.

[26] A. Vogel, A. Drews, T. Kamionka, M. Bolte, and G. Meier, "Influence of dipolar interaction on vortex dynamics in arrays of ferromagnetic disks," *Phys. Rev. Lett.*, vol. 105, no. 3, p. 037201, Jul. 2010.

[27] S. Sugimoto, Y. Fukuma, S. Kasai, T. Kimura, A. Barman, and Y. Otani, "Dynamics of coupled vortices in a pair of ferromagnetic disks," *Phys. Rev. Lett.*, vol. 106, no. 19, p. 197203, May 2011.

[28] K. S. Buchanan *et al.*, "Soliton-pair dynamics in patterned ferromagnetic ellipses," *Nature Phys.*, vol. 1, no. 3, pp. 172–176, Dec. 2005.

[29] P. Vavassori, N. Zaluzec, V. Metlushko, V. Novosad, B. Ilic, and M. Grimsditch, "Magnetization reversal via single and double vortex states in submicron Permalloy ellipses," *Phys. Rev. B, Condens. Matter*, vol. 69, p. 214404, Jun. 2004.

[30] T. Zeng, Y. Zhou, K.-W. Lin, P.-T. Lai, and P. W. T. Pong, "Magnetic-field-sensing mechanism based on dual-vortex motion and magnetic noise," *J. Appl. Phys.*, vol. 115, no. 17, p. 17D142, May 2014.

[31] M. J. Donahue and D. G. Porter, "OOMMF user's guide," Nat. Inst. Standards Technol., Gaithersburg, MD, USA, Interagency Rep. NISTIR 6376, 1999.

[32] L. D. Landau and E. Lifshitz, "On the theory of the dispersion of magnetic permeability in ferromagnetic bodies," *Phys. Z. Sowjetunion*, vol. 8, no. 153, pp. 101–114, 1935.

[33] T. L. Gilbert, "A Lagrangian formulation of the gyromagnetic equation of the magnetization field," *Phys. Rev.*, vol. 100, p. 1243, 1955.

[34] J. Lee, K. Oh, H.-J. Kim, and K. Y. Kim, "Magnetization reversal process of the nanosized elliptical permalloy magnetic dots with various aspect ratios," *J. Magn. Magn. Mater.*, vols. 272–276, pp. 736–737, May 2004.

[35] K. S. Buchanan *et al.*, "Magnetization reversal in patterned double-vortex structures," *J. Appl. Phys.*, vol. 97, no. 10, p. 10H503, May 2005.

[36] M. Rahm *et al.*, "Vortex nucleation in submicrometer ferromagnetic disks," *Appl. Phys. Lett.*, vol. 82, no. 23, pp. 4110–4112, Jun. 2003.

[37] T. Okuno, K. Shigeto, T. Ono, K. Mibu, and T. Shinjo, "MFM study of magnetic vortex cores in circular permalloy dots: Behavior in external field," *J. Magn. Magn. Mater.*, vol. 240, nos. 1–3, pp. 1–6, Feb. 2002.

[38] M. Schneider, H. Hoffmann, and J. Zweck, "Lorentz microscopy of circular ferromagnetic permalloy nanodisks," *Appl. Phys. Lett.*, vol. 77, no. 18, pp. 2909–2911, Oct. 2000.

[39] A. Krichevsky, M. Belov, and M. R. Freeman, "The evolution of dynamic switching diagrams of small Permalloy ellipses with magnetic field pulse duration," *J. Magn. Magn. Mater.*, vol. 301, no. 1, pp. 181–189, Jun. 2006.

[40] K. Y. Guslienko, K.-S. Lee, and S.-K. Kim, "Dynamic origin of vortex core switching in soft magnetic nanodots," *Phys. Rev. Lett.*, vol. 100, no. 2, p. 027203, Jan. 2008.